



# Bi<sub>2</sub>MoO<sub>6</sub> nanofilms on the stainless steel mesh by PS-PED method: Photocatalytic degradation of diclofenac sodium as a pharmaceutical pollutant

Mahboobeh Zargazi<sup>a</sup>, Mohammad H. Entezari<sup>a,b,\*</sup>

<sup>a</sup> Sonochemical Research Center, Department of Chemistry, Faculty of Science, Ferdowsi University of Mashhad, Mashhad, Iran

<sup>b</sup> Environmental Chemistry Research Center, Department of Chemistry, Faculty of Science, Ferdowsi University of Mashhad, Mashhad, Iran

## ARTICLE INFO

### Keywords:

Bi<sub>2</sub>MoO<sub>6</sub> film  
Sonelectrodeposition  
Pulse mode  
Photocatalytic degradation  
Diclofenac sodium

## ABSTRACT

For the first time, Bi<sub>2</sub>MoO<sub>6</sub> nanofilms were successfully synthesized by simultaneous pulse sonication-pulse electrodeposition (PS-PED) on the stainless steel mesh surface. Bismuth molybdate films were formed under various combinations of electrodeposition and sonication (sono-electrodeposition) in continuous and pulse modes. Porous Bi<sub>2</sub>MoO<sub>6</sub> films synthesized by PS-PED method and showed the highest efficiency in photocatalytic degradation in comparison with other films. Bi<sub>2</sub>MoO<sub>6</sub> film obtained from PS-PED had a thickness of 13.78 nm while, the thickness for the electrodeposition method was 39.52 nm. The high photocatalytic efficiency is attributed to the high surface roughness and low thickness of film synthesized by PS-PED method. Indeed, ultrasound played a key role in the synthesis of films with high surface roughness. On the other hand, shock waves and micro-jets could be dissolved diffusion problems and reduced the dendrite like structures in deposition process. Simultaneous application of pulse modes for both combined methods led to more growth of crystallographic planes. This is due to reaction of ions on the surface in interval relaxation times and produce more nuclei for growth. In order to obtain a high efficiency, response surface methodology was used for optimization of effective variable parameters ( $t_{on}$ ,  $t_{off}$  and sonication amplitude) in film preparation.

## 1. Introduction

In recent years, the presence of pharmaceutical residues in the water sources has converted to major challenges in point of the environmental remediation [1–3]. Indeed, pharmaceutical pollutants such as antibiotics [4], antidiabetics [5], and X-ray contrast media [6,7] are incompletely metabolized by the human or animal and transferred to water resources. Diclofenac, Ibuprofen, Ketoprofen, and Naproxen are commonly indicated drugs spread to environment via human and animal feces due to their large consumption [8–10]. Since these pharmaceuticals have long half-lives in the environment, they frequently accumulate and reach to biologically active levels. Diclofenac [2-(2,6-dichloranilino) phenylacetic acid], an anti-inflammatory drug which greatly used in all over the world is one of the most commonly detected dangerous pollutants in wastewater [11]. Research indicates that it has the potential to bio-accumulate in the tissues of organisms [12,13]. Other studies reported the presence of 1 ppb of diclofenac could damage liver and kidney cell functions in aquatic animals [14,15].

Heterogeneous photocatalysts offer high potential for converting visible light energy into active chemical species for decomposing of organic pollutants [16–18]. As an example, TiO<sub>2</sub>-based photocatalysts used for purification of air and water. However, the band gap of TiO<sub>2</sub> is 3.2 eV, which means it can only illustrate activity under UV irradiation [19]. The low quantum efficiency of TiO<sub>2</sub> remains another limiting factor to use of photocatalytic materials based on TiO<sub>2</sub>. Conventional methods, such as doping with another elements [20] or photosensitization [21], only partially solve this issue. There is an observable need for the improvement of visible light activated low band gap semiconductors, thus providing an environmentally friendly solution for air and water detoxification processes.

Bismuth complex oxides are often referred to as examples of efficient visible light activated photocatalytic materials with narrow band gap [22,23]. Bismuth molybdate and bismuth tungstate being the most investigated members of the bismuth complex oxides family [24,25]. Bismuth molybdate is an Aurivillius family with formula Bi<sub>2</sub>MoO<sub>6</sub>, it is well defined in the literature due to its remarkable physical and

\* Corresponding author at: Sonochemical Research Center, Environmental Chemistry Research Center, Department of Chemistry, Faculty of Science, Ferdowsi University of Mashhad, Mashhad, Iran.

E-mail address: [entezari@um.ac.ir](mailto:entezari@um.ac.ir) (M.H. Entezari).

<https://doi.org/10.1016/j.ultsonch.2019.104867>

Received 3 February 2019; Received in revised form 13 September 2019; Accepted 7 November 2019

Available online 09 November 2019

1350-4177/ © 2019 Elsevier B.V. All rights reserved.

chemical properties [26]. It finds applications as a gas sensor [27], dielectric [28], and has recently been reported as an efficient visible light-activated photocatalyst [29,30]. The interest in bismuth-based photocatalysts arises from the low band gap values, as the result of hybridization between the Bi2s and O2p states. Photocatalytic bismuth molybdates are typically synthesized using chemical methods, such as the hydrothermal method [30], molten salt method [31], sol-gel reaction [32] or the Pechini method [33]. Very few data are available on the photocatalytic behavior of thin films of bismuth compounds such as Bi<sub>2</sub>WO<sub>6</sub> [34], BiFeO<sub>3</sub> [35] and Bi<sub>2</sub>MoO<sub>6</sub> [29]. To date, various methods have been reported for the synthesis of thin films of bismuth molybdate such as sputtering [36], physical deposition methods [37] and electrodeposition [38]. Pulsed electrodeposition (PED) is a technique that has recently gained much attention for deposition of nanometals onto conductive surfaces or nanocarbon defect sites. With PED, a high overvoltage (high current density) is used in the same fashion as classic electrodeposition (ED), but the driving potential is applied for short time period. During the relaxation period (i.e., non-plating period time), dissolved metal ions migrate to the surface where ion consumption is highest (i.e., high local current density), resulting in a more uniform distribution of metal nanoparticles compared to standard potentiostatic or galvanostatic ED. One of the most common problems with ED is uncontrolled “overgrowth” of dendritic structures beyond the working diameter of the electrode. Another technique used to synthesize metal nanoparticles is sonochemical electrodeposition (SED). SED combines galvanostatic or potentiostatic ED with sonication. SED reduces diffusion limitations by facilitating acoustic cavitation and microjet effects at the surface of the nucleating metal structure. In addition, destabilizing bubbles formed during the deposition process provide some convective mixing of dissolved metal ions within the mass boundary layer. However, SED still hampered by diffusion limitations to the surface and there is no demonstration over nanoparticle size control. To date, no previous methodologies have combined PED and SED using a bimodal pulsing strategy for deposition of nanometal onto electrodes. Here, this study developed the combination of these two techniques, called pulsed sono-pulsed electrodeposition (PS-PED), and demonstrate deposition of ultra-thin film Bi<sub>2</sub>MoO<sub>6</sub> (BMO) on the stainless steel mesh as substrate for the first time. Stainless steel mesh chosen as substrate for several reasons such as low cost, webbed structure, mechanical and chemical stability. Webbed structure of substrate affected the harvesting and multi-scattering of visible light compared to common stainless steel. The as-synthesized large-area BMO films show predominant photocatalytic performances in comparison with ED method for degradation of Diclofenac (DCF). Effective variables in synthesis of films optimized by response surface method.

## 2. Experimental

### 2.1. Materials and experiment

All reagents were of analytical grade and used directly without any purification. Bismuth molybdate thin film prepared by various combination of two methods of electrodeposition and sonodeposition in a convectional three electrodes cell with ultrasonic probe. A graphite plate with surface area about 4 cm<sup>2</sup> was used as the auxiliary electrode, a saturated Ag/AgCl electrode was used as a reference electrode and stainless steel mesh about 2 cm<sup>2</sup> was used as a working electrode. Prior to deposition, stainless steel mesh was cleaned ultrasonically in acetone, ethanol and finally in deionized water. The electrolyte solution contained an aqueous solution of 0.01 molL<sup>-1</sup> Bi(NO<sub>3</sub>)<sub>3</sub>·9H<sub>2</sub>O, 0.1 molL<sup>-1</sup> Na<sub>2</sub>MoO<sub>4</sub>·2H<sub>2</sub>O with 0.1 molL<sup>-1</sup> Na<sub>2</sub>EDTA as a complexing agent. Deposition carried out by different methods shown in Table 1. Selected potential and transferred charge in cathodic electrodeposition are -2 V and 696 C, respectively. Electrodeposition under potentiostat was named ED, pulsed electrodeposition was denoted PED. SED, SPED,

**Table 1**  
Different methods used for deposition of BMO film.

Method	Electro-characteristics		Sono-characteristics	
	Potential(V)	t <sub>on</sub> /t <sub>off</sub> (s/s)	Amplitude	t <sub>on</sub> /t <sub>off</sub> (s/s)
ED	-2	...	...	...
PED	-2	4/8	...	...
SED	-2	...	30%	...
SPED	-2	4/8	30%	...
PSED	-2	...	30%	4/8
PSPED (1) *	-2	4/8	30%	4/8
PSPED (2) **	-2	4/8	30%	4/8(off/on)

\*: at t<sub>on</sub> ED, sono is on \*\*: at t<sub>on</sub> ED, sono is off.

PSED and PSPED referred to sonoelectrodeposition, sono-pulse electrodeposition, pulse sono-electrodeposition, and pulse sono-pulse electrodeposition, respectively. Ultrasonic horn (BRANSON, digital Sonifier 450, and 20 kHz) with intensity of 18 W/Cm<sup>2</sup> measured by thermal method [39] and used as a sonication source. To show the effect of ultrasound, BMO films synthesized by cyclic voltammetry (CV) in the presence and absence of ultrasound. The scan rate and cycle number were 0.2 (V/s) and 80 cycles, respectively. Ultrasound used in continuous and pulse modes with 40% amplitude and the films named by CV (US, C) and CV (US, P) expressions, respectively. Furthermore, the sample prepared in the absence of ultrasound depicted by CV. Schematics in Fig. 1 show the required set ups for deposition of films.

### 2.2. BMO thin film characterization

To characterize the BMO thin films, X-ray powder diffraction were performed on a XRD, Explorer GNR Italia under a Dectris diffract meter employing Cu K $\alpha$  radiation,  $\lambda = 1.5418 \text{ \AA}$ . The morphology and size of the as-prepared films characterized by using a scanning electron microscope (SEM, LEO, Germany) equipped with EDX (EDS, Inca-350, Oxford instruments) which was applied for elemental analysis of thin films. Thin film thickness and surface roughness evaluated by Atomic Force Microscopy (AFM) analysis. UV-Visible Diffuse reflectance spectroscopy (Avaspec 2048 Tech) used for band gap determination.

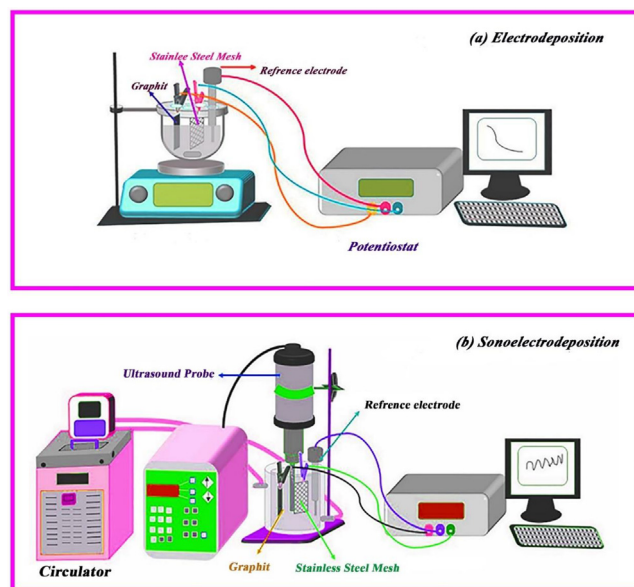


**Fig. 1.** Schematics depict synthesis process by (a) electrodeposition and (b) sonoelectrodeposition.

### 2.3. Photocatalytic activity of BMO thin films

The photocatalytic activity of BMO thin films was evaluated with DCF (10 ppm) as a pharmaceutical pollutant model in our designed photocatalytic setup [34] under natural sunlight. The process of photocatalytic degradation monitored by withdrawing definite volume of aqueous solutions at certain interval times and measured the absorbance by UV-Vis spectrophotometer (Unique 2008). Before illumination, to reach an adsorption and desorption equilibrium between film and pollutant, the system rotated in dark for 2 h. The concentration of DCF samples during the illumination followed through the calibration curve. Furthermore, the photocatalytic properties of films prepared by CV, CV (US, C) and CV (US, P) evaluated for degradation of DCF. CV and Linear sweep voltammetry (LSV) studies were investigated for all samples in Na<sub>2</sub>SO<sub>4</sub> (0.1 M) as electrolyte in the dark and light. The photoelectrochemical studies carried out by SAMA 500 Electrochemical Analyzer and Xe lamp (55 W). Electrochemical Impedance spectroscopy (EIS) used for evaluation of recombination rate of photogenerated hole/electrons. EIS analysis conducted in a perturbation voltage of 10 mV amplitude over the frequency range of 10<sup>2</sup>–10<sup>5</sup> Hz by Auto lab (302n, Poland).

### 2.4. Central composite design (CCD)

After finding BMO thin film with high degradation efficiency, the central composite design (CCD) applied to investigate the effects of the three independent variables on the response function. The independent variables are shown as On time ( $X_1$ ), Off time ( $X_2$ ) and Sonication amplitude ( $X_3$ ). The levels of the three selected major factors summarized in Table 2. The notations (–1), (0) and (+1) refer to the low, medium, and high levels of independent variables in experimental design, respectively. In developing the regression equation developed by Box-Hunter, the test factors coded according to the following equation:

$$X_i = \frac{(X_i - X_0)}{\Delta X_i} \quad (1)$$

where  $X_i$  is the dimensionless value of an independent variable,  $x_i$  represents the real value of the independent variable,  $x_0$  is the real value of the independent variable at the center point, and  $\Delta x_i$  is the step change.

$$Y = b_0 + \sum_{i=1}^k b_i X_i + \sum_{i=1}^k b_{ii} X_i^2 + \sum_i \sum_j b_{ij} X_i X_j + \varepsilon \quad (2)$$

where  $Y$  is the predicted response,  $b_0$  is the offset term,  $b_i$  is the linear effect,  $b_{ii}$  is the squared effect and  $b_{ij}$  is the interaction effect. To elucidate the influence of pulse time, herein composite central design was applied to design experiments with different parameters such as  $t_{on}$ ,  $t_{off}$  and sonication amplitude.

## 3. Results and discussion

### 3.1. Characterization of Bi<sub>2</sub>MoO<sub>6</sub> film

The best film (PS-PED (1)) with highest degradation efficiency for DCF selected for characterization. Furthermore, another film synthesized by ED method also characterized for comparison studies. The XRD patterns of films depicted in Fig. 2 and the peaks in films indexed as

**Table 2**  
Independent variables and their coded levels.

Symbol	Parameters	Coded levels		
		–1	0	+1
X1	$t_{on}$ (Sec)	4	8	12
X2	$t_{off}$ (Sec)	4	8	12
X3	Sonication amplitude (%)	20	40	60

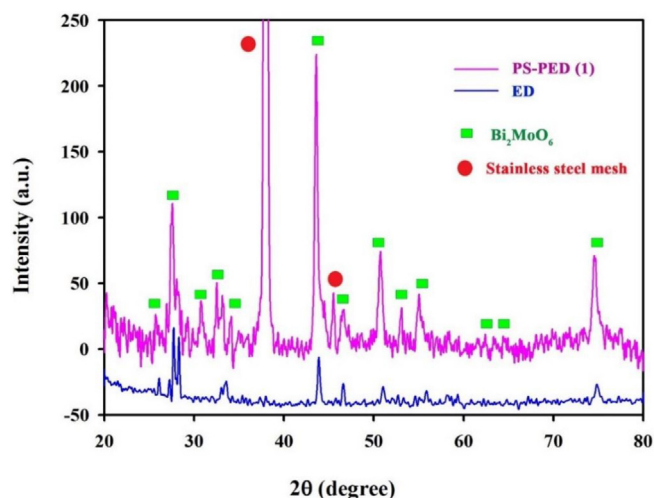


Fig. 2. XRD pattern for both BMO films.

(ICCD database, NO. 00-033-0208). The film synthesized by PS-PED method shows high growth crystallite plates in comparison with ED method. It attributed to the presence of ultrasonic waves that produced more nucleation and led to growth of plate in some directions. Crystallite size measured for samples prepared by ED and PS-PED methods through Scherrer equation and they were 45.9 and 22.3 nm, respectively.

Shapes and morphology of films presented by SEM images in Fig. 3. The film synthesized by PS-PED method in Fig. 3b shows high homogeneity compared to film by ED method in Fig. 3a. Furthermore, SEM image in Fig. 3b indicated very tiny whiskered structures on the film surface. Whereas, ED method produces film with cumulative growth structure (Fig. 3a and 3c) and cracked structure (in Fig. 3e). On the other hands, film by PS-PED indicates single shape with very tiny whiskers and voids on its surface (Fig. 3d, f). Elemental dispersive X-ray (EDS) analysis used for determining of the presence of elementals in

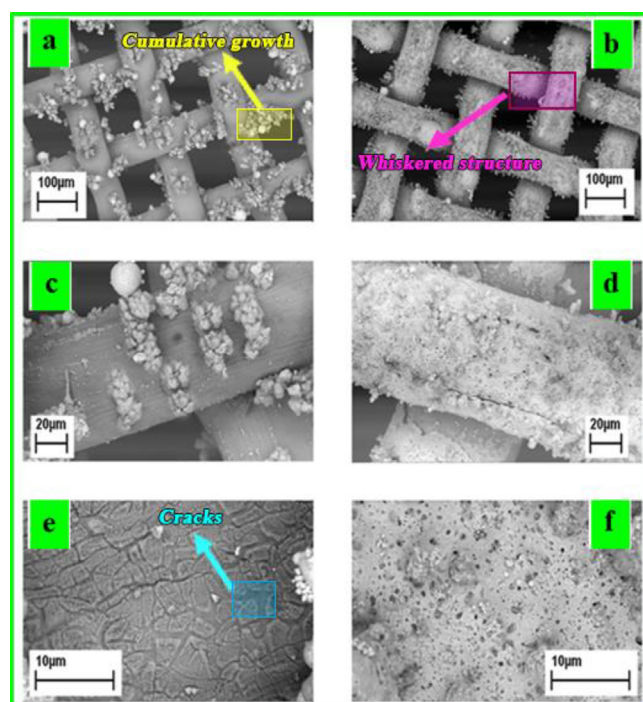


Fig. 3. SEM images for BMO films synthesized by ED (a,c,e) and PS-PED (b,d,f) methods at various magnification.

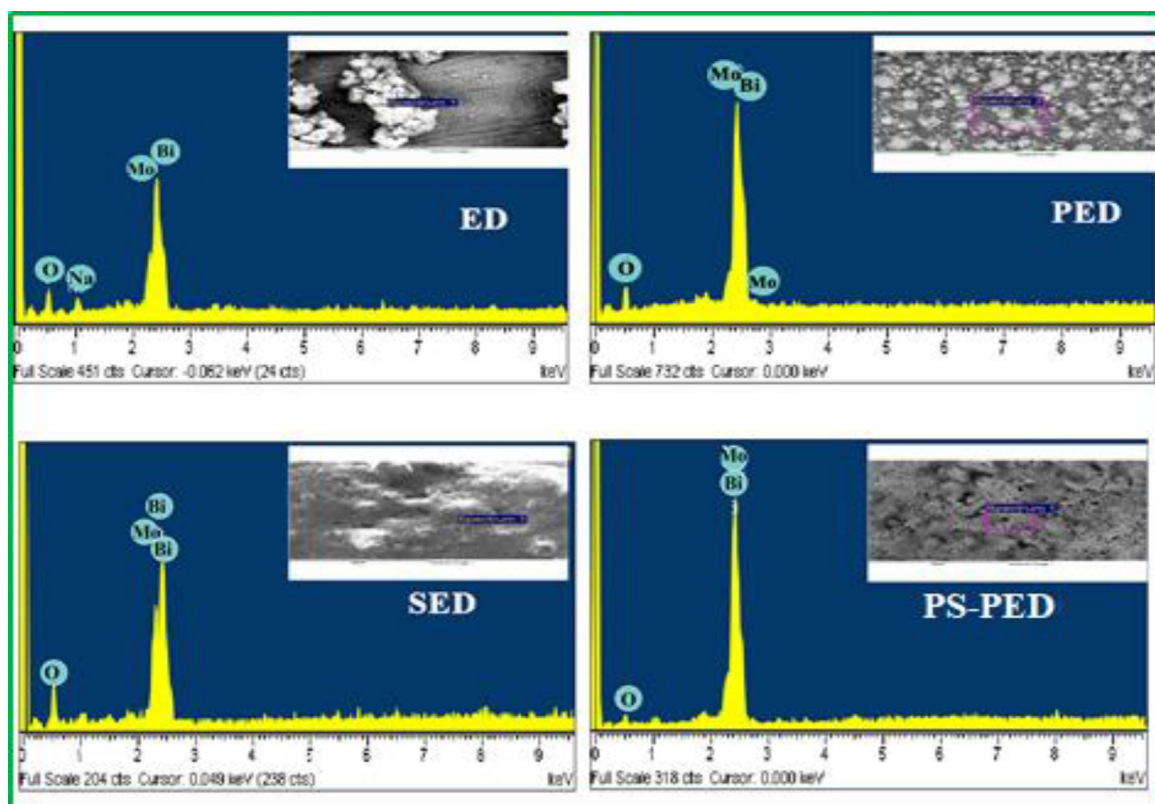


Fig. 4. EDS analysis related to films synthesized by ED, PED, SED and PS-PED methods.

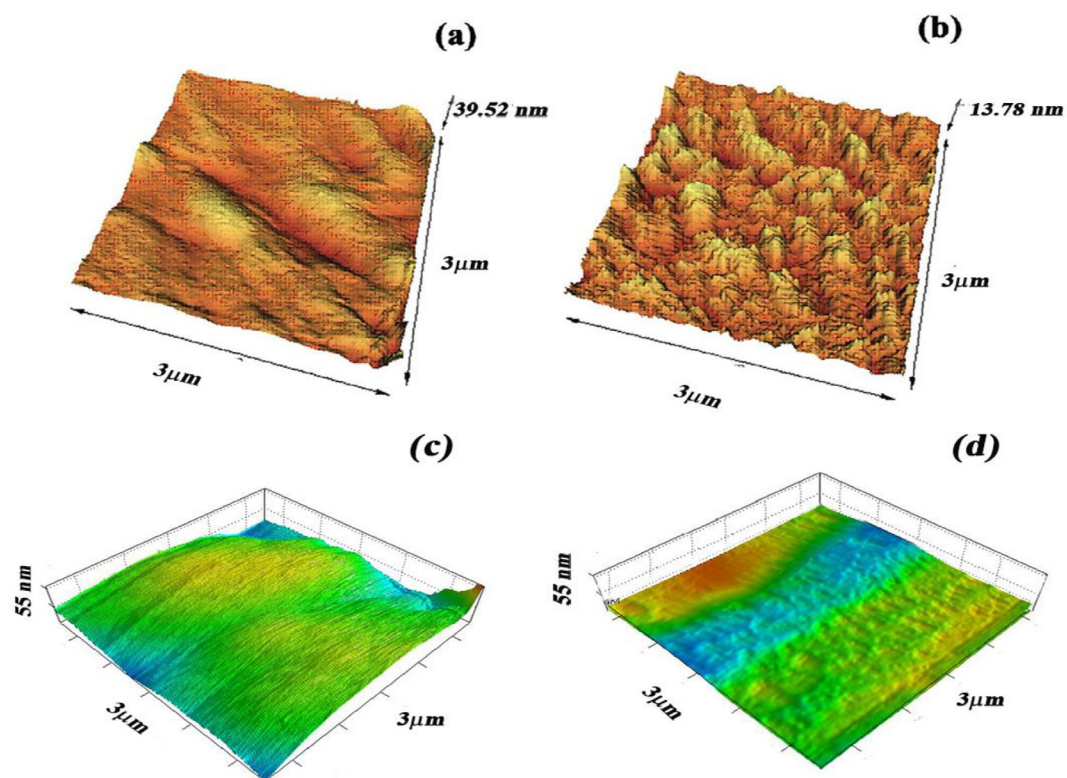


Fig. 5. 3D-AFM images for film synthesized by (a) ED, (b) PS-PED and 3D images with same Z axes for (c) ED, (d) PS-PED.

films synthesized by ED, PED, SED and PS-PED methods. Based on the results obtained in Fig. 4, Bi, Mo and O elements were appeared in all EDS spectra for four samples. The peak intensity of elements at

individual samples is different. For instant, film by PS-PED shows high peak intensity for high weight elements Bi and Mo due to throwing effect of ultrasound for ions from bulk to surface electrode. About PED

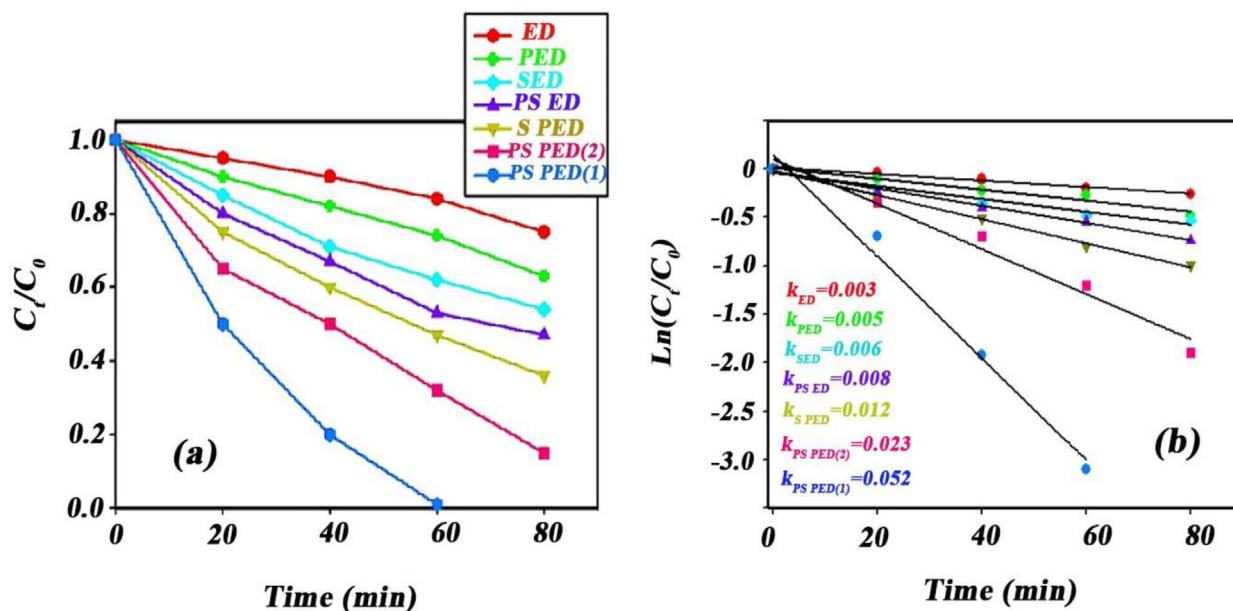


Fig. 6. (a) photocatalytic degradation of DCF by different films, (b) kinetic studies of obtained experimental data.

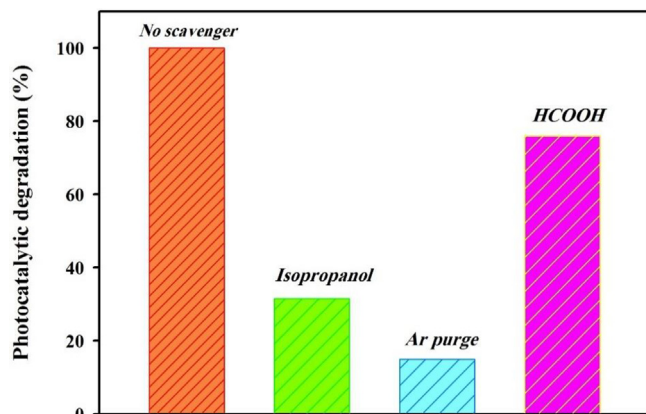


Fig. 7. photocatalytic degradation of DCF in the presence of scavengers.

and SED methods, it is important that the relaxation time and sonication waves have main roles in peak intensity, respectively. Morphology of films determined by AFM images in Fig. 5. Film synthesized by PS-PED method (Fig. 5b) has higher surface roughness in comparison with film synthesized by ED method (Fig. 5a). At the same Z-axis showed in Fig. 5c,d, different surface morphologies and thickness were presented for films. The thickness of film by PS-PED method was about 13.78 nm that is smaller than the film by ED with 39.52 nm.

### 3.2. Photocatalytic activities of BMO films

All of the synthesized BMO films were applied for photocatalytic degradation of DCF in an aqueous solution. Based on Fig. 6a, the film obtained from PS-PED (1) was demonstrated the highest activity than other films and DCF can be degraded completely in 60 min. But, the degradation of DCF by the sample prepared by PS-PED (2) method was longer than PS-PED (1) method. The high efficiency can be justified by the structure of films obtained from both methods. In the case of PS-PED (1), electrodeposition and sonication are in the pulse positions and simultaneously are in an On time and Off time. These conditions lead to throw of high weight elements by ultrasound from bulk to electrode surface and diminish problems of diffusion in ED. In the case of PS-PED (2), if PED is at  $t_{on}$ , PS is at  $t_{off}$  and vice versa. Therefore, during PED at

$t_{on}$ , deposition performed by ED alone. At relaxation time of (PED),  $t_{off}$ , PS is at  $t_{on}$ , and under this condition, ultrasound decreased the dendrite like structures besides dissolving of structure formed in relaxation time of PED. Finally, the layer was smoother than layer obtained from PED alone and the coverage of substrate was lower than PS-PED (1).

The rate of photocatalytic degradation of DCF was exhibited in Fig. 6b for all mentioned processes. The results confirmed that the photocatalytic efficiency for PS-PED (1) is higher than other methods. Furthermore, to determine kinetic order of photocatalytic processes, first-order and second-order studies were evaluated for prepared films for degradation of DCF. The results were confirmed better with first-order kinetic model than second-order. DRS UV-Vis spectrum for PS-PED (1) sample presented in Fig. 1S and it confirmed that the sample has an adsorption in visible region. The band gap of sample is 2.68 eV and it demonstrates a visible-light photocatalytic activity. Cyclic voltammograms of samples in dark and under visible light showed in Fig. 2S and the results approved a high photocurrent efficiency for PS-PED (1) sample compared to other samples. LSV curves also confirmed a high photocurrent for PS-PED (1) sample in comparison with other samples. These results suggested that ultrasound has major effects in the formation of film (see Fig. 3S). In the dark, higher current can attribute to higher amount of deposited film. There is no photocurrent in CV and LSV tests for the bare substrate. EIS analysis for two selected samples (ED, PS-PED (1)) evaluated in dark and under light irradiation. Nyquist curves (Fig. 4S) exhibited different behaviors for samples in dark and light in the presence and absence of DCF. The small radius of semicircles under light confirmed the low rate of recombination of hole-electrons in the photo-induced processes. In the presence of DCF under light, semicircles for both films have smaller radius than in the absence of DCF due to the capture of photogenerated holes on the surface films by DCF molecules that lead to reduce of recombination rates. It was clearly shown in Fig. 4S that PS-PED film indicated higher separation photogenerated holes and electrons in the presence of DCF than ED film. Large semicircles for samples in the dark, related to capacity and resistance of film in the electrolyte. Furthermore, photocatalytic efficiencies of samples prepared by CV, CV (US, C) and CV (US, P) also depicted in Fig. 5S. High degradation efficiency exhibited for CV (US, C) sample in comparison with other samples. The main reason for this behavior attributed to high amount of deposited photocatalyst on the substrate. Continuous sonication produced thicker film due to sonication effect in throwing of ions to double layer and creation higher

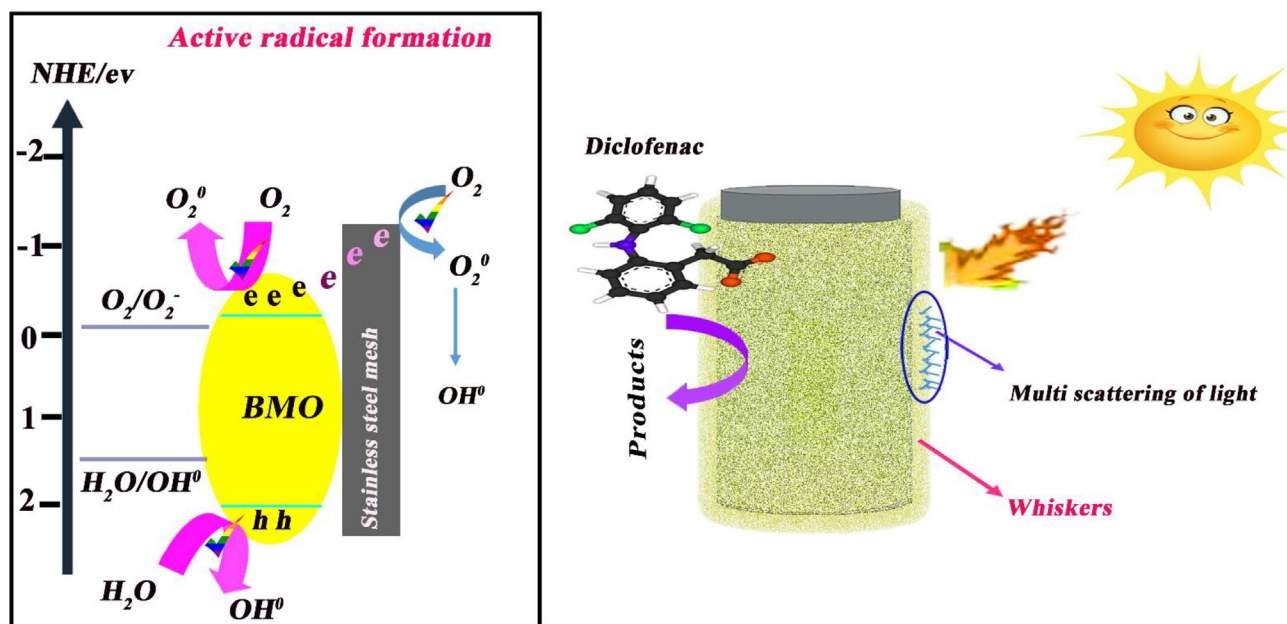


Fig. 8. Proposed mechanism for photocatalytic activity of BMO film (PS-PED).

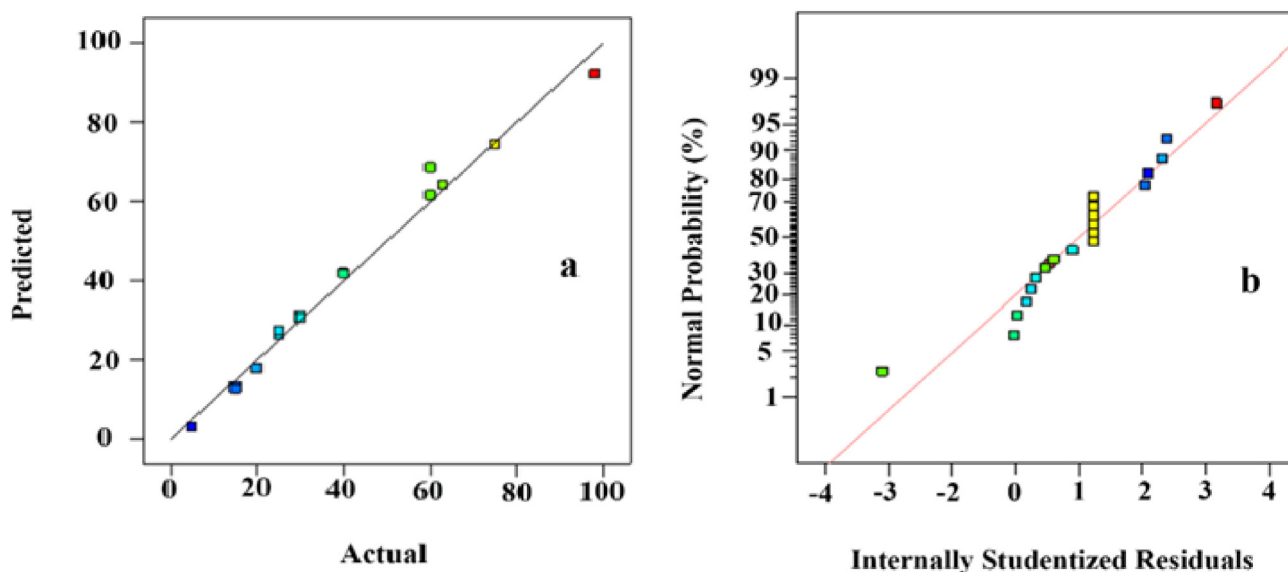


Fig. 9. (a) predicted values obtained from model versus experimental values and (b) normal probability plotted against internally studentized residuals.

nucleation than CV and CV (US, P) methods. Cyclic voltammograms and LSV curves confirmed the production of photocurrent due to accumulation of photogenerated electrons under visible light irradiations (see Fig. 6S). Based on the mentioned results, to gain a high photocatalytic efficiency, optimization by CCD carried out on the effective independent parameters in the synthesis of films by PS-PED (1) method.

### 3.3. Proposed mechanism for photocatalytic activity of BMO film (PS-PED)

Various scavengers applied for identifying photocatalytic degradation mechanism of DCF on the BMO film prepared by PS-PED method. Isopropanol and formic acid applied as OH radical and hole quenchers during the photocatalytic process. The effect of oxygen also investigated by Ar gas purging in photocatalytic reactor. Based on the results depict in Fig. 7, OH radicals and the presence of oxygen have high effects in photocatalytic degradation.

Schematic in Fig. 8 shows that film has a very tiny whiskered

structure that acted as sites for trapping and multi-scattering of visible light. Furthermore, under irradiation of light, the photogenerated electron-hole interacted with adsorbed oxygen and water molecules to produce active radicals ( $\text{OH}^\bullet$  and  $\text{O}_2^\bullet$ ). It observes that the photogenerated hole-electrons have appropriated energy levels for oxidation of water and  $\text{O}_2$  reduction. Whiskered structures provided very tiny routs for electron transferring hence has a key role in separation of charged pairs. Finally, the photogenerated electrons could be captured by conductive substrate and prevented from fast recombination of electron-hole. Ultra-thin thickness of film suggested that substrate has a high effect in separation and electron transferring due to short diffusion routs of electrons.

### 3.4. Statistical analysis

To get a high performance, the effective parameters in film synthesis process was optimized by CCD and 20 designed experiments were

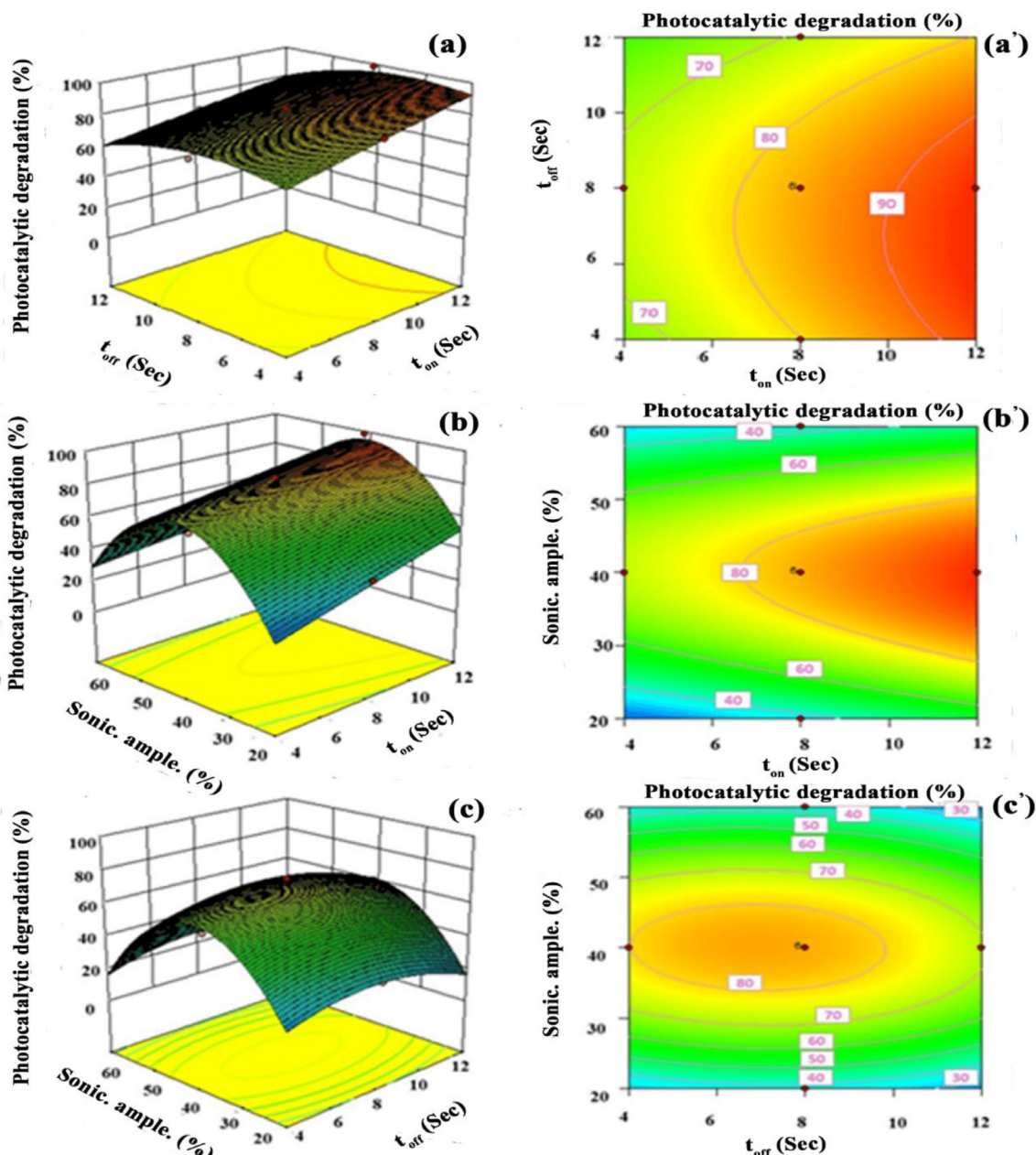


Fig. 10. 3-D curves and counter maps presented (a,a') the effect of  $t_{on}$  and  $t_{off}$ , (b,b') the effect of  $t_{on}$  and sonication amplitude and (c,c') the effect of  $t_{off}$  and sonication amplitude on the photocatalytic degradation (%).

proposed for the response surface modeling (Table 1S). The best performance of films obtained at 30 min. Therefore, the photocatalytic efficiency for other films investigated in the period of 30 min. According to the experimental design, a polynomial equation calculated for actual parameters that empirically indicated dependence of response to variable factors (Eq. (3)).

$$\begin{aligned} \text{Degradation (\%)} &= +85.33636 + 10.05X_1 - 3.5X_2 + 0.5X_3 - 2.25X_1X_2 - 3.5X_1X_3 - 2.75X_2 \\ &X_3 - 1.34091X_1^2 - 4.09091X_2^2 - 52.09091X_3^2 \end{aligned} \quad (3)$$

To assess the model adequacy, analysis of variance (ANOVA) extracted and examined. According to the ANOVA of the polynomial model (Table 2S), the F-value and P-value for the model is 235.01 and < 0.0001 respectively, confirming that the applied model is significant. The F-value of "lack-of-fit" is 1.05 that indicates the lack of fit is not significant. P-value of "lack of fit" stated that there is only

13.46% probability for the lack of fit due to the noise. Successful prediction of proposed model confirms by the non-significant lack of fit. The accuracy of the model depicts in Fig. 9, and compares the actual values against the predicted responses of the model for the degradation of DCF (Fig. 9a). The normal probability curve in Fig. 9b proved the normal distribution and independent of errors with homogeneous variances.

In this work, the independent factors including  $t_{on}$  ( $X_1$ ),  $t_{off}$  ( $X_2$ ), and the second-order effect of  $t_{off}$  ( $X_2^2$ ) and sonication amplitude ( $X_3^2$ ) considered significant variables with p-value < 0.001. Furthermore, the interaction effect of  $t_{on}$  and sonication amplitude ( $X_1X_3$ ) are significant at  $p < 0.05$ . The negative and positive coefficients of the terms in the polynomial expression suggest their negative and positive effects on photocatalytic efficiencies, respectively. Moreover, the value of  $p > 0.05$  means that the model parameters are insignificant. In accordance with p values in ANOVA  $p(X_1) = < 0.0001$ ,  $p(X_2) = 0.0004$  and  $p(X_3) = 0.7359$ . Thus, the importance of factors in

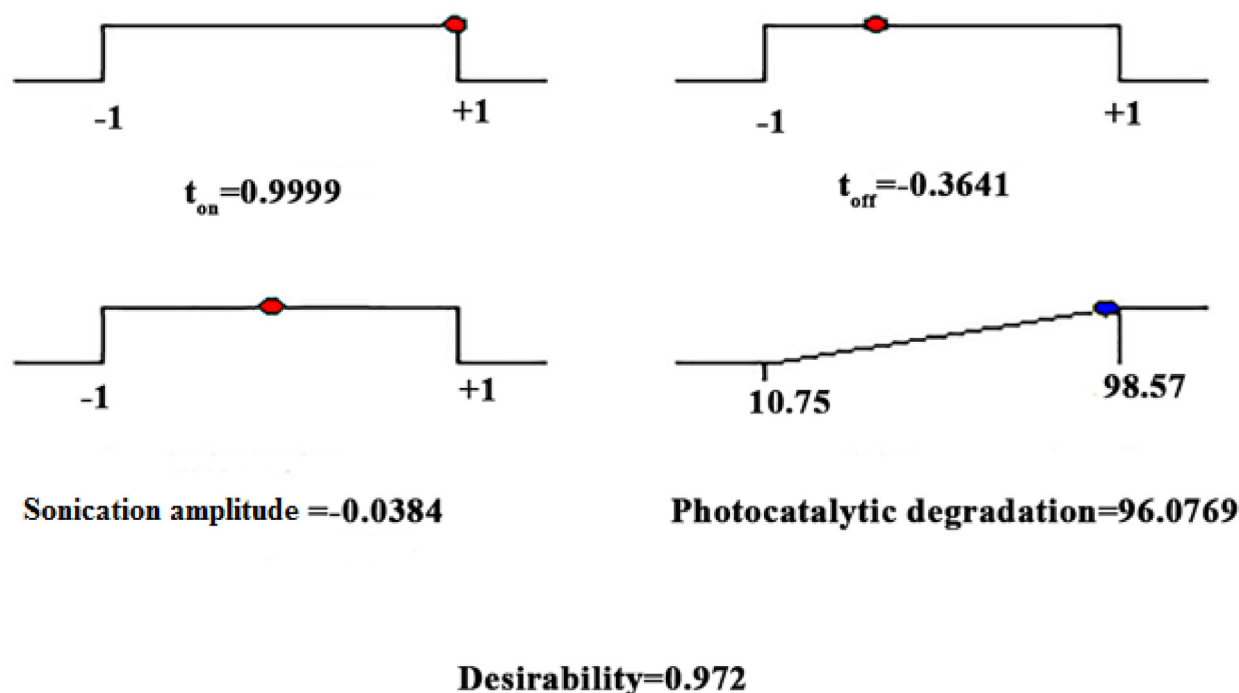


Fig. 11. Ramps for numerical optimization.

film synthesis process is as follows:  $t_{on} > t_{off} >$  sonication amplitude. These results related to the chosen ranges of experimental variables in this study.

### 3.5. Response surface analysis

3-D curves and counter maps demonstrated to determine the optimum values of two parameters at medium value of the third parameter. The interactions between the three independent factors and the response depicted in Fig. 10. Based on Fig. 10a, the photocatalytic degradation efficiency increases with increasing  $t_{on}$  but different behavior observed for  $t_{off}$  parameter. First, degradation efficiency increased with increasing of  $t_{off}$  and then decreased. These results were confirmed by counter map in Fig. 10a'. This behavior attributed to the deposition yield in coating of the substrate. Deposit yield increased with increasing  $t_{on}$  due to more nucleation while  $t_{off}$  has critical value. Deposit yield increased until 8 s and then decreased. This is due to high relaxation time ( $> 8$  s) which led to more dissolving of produced films in previous step. Fig. 10b, also depicts simultaneous effects of  $t_{on}$  and sonication amplitude on the response. Degradation efficiency enhanced smoothly with an increase in sonication amplitude from 20 to 40% and then decreased gradually when the sonication amplitude reach to 60% whether  $t_{on}$  has a low or high value. The positive effect of sonication amplitude attributed to the influence of sonication power in throwing of ions to double layer to produce more nucleation and inhabit from creation of the dendrite like structures. While negative effect related to the high ultrasonic amplitude that may led to detach of films from the substrate. Fig. 10b' shows the counter maps for the interaction between two variables by using color intensities. High color intensity indicated positive parameter effect on the surface response. The influence of interaction between two variables ( $t_{off}$  and sonication amplitude) on the photocatalytic degradation shown by 3D curves in Fig. 10c. The obtained results suggested different behaviors for two parameters. Both  $t_{off}$  and sonication amplitude have critical values due to their negative effects on the deposit yield. Counter map in Fig. 10c' also shows that the low color intensity represented the low concurrent influence of two parameters on the surface response. On the other hands, the low number of circles in the counter maps indicated high interaction

between two parameters and this matches with values in ANOVA table. As a result, the interaction effect between  $t_{on}$  and sonication amplitude on the surface response is more effective than other interaction effects.

### 3.6. Optimization of effective variables

Optimal values obtained from base of desirability function for photocatalytic degradation of DCF. Maximum desirability gets by numerical calculations that denoted by the specific point. The criteria for all factors in correspondence with degradation efficiency depicted in Table 3S. The weight and importance give added emphasis to upper or lower bounds and target values, respectively. As the high degradation yield is the main objective for such studies, an "importance" value of 5 was considered the maximum goal. On the basis of the above limitations and numerical calculations, the optimum conditions for maximum DCF degradation efficiency (98.57%) were found to be at  $t_{on}$  value of high level (+1), at  $t_{off}$  value of below medium level ( $-0.36$ ) and at sonication amplitude value of medium level ( $-0.03$ ) with high desirability of 0.972 (Fig. 11).

### 3.7. Model's validation

To confirm validation of model, the value of the determination coefficient ( $R^2 = 0.9953$ ) depicted in Table 4S. This suggested that 99.53% of the variability in the response surface could explain by the model. Also, the adjusted coefficient ( $R^2 = 0.9911$ ) is high and confirming that the obtained model is significant. If, the value of coefficient of variance (CV) is smaller than 10%, it shows that the model is reproducible. For this study, CV value of 4.91% demonstrated low deviation between experimental and predicted values. Parameter of adequate precision (AP) calculated the signal to noise ratio, and should be higher than 4 for the model. The calculated AP value of 43.183 shows an adequate precision discrimination for proposed model. Furthermore, the value of adjusted- $R^2$  is close to predicted- $R^2$  value (0.9360), indicating a good relation between experimental and predicted values.

#### 4. Conclusion

In this work, for the first time, the nanofilm of  $\text{Bi}_2\text{MoO}_6$  with whiskered-like structures were successfully synthesized by PS-PED method. The influence of pulse parameters ( $t_{\text{on}}$  and  $t_{\text{off}}$ ) and sonication amplitude were studied in the film synthesis process. The response surface method used for optimization of these parameters. The film prepared by PS-PED method was applied for photocatalytic degradation of diclofenac sodium as a pharmaceutical pollutant. In comparison with ED alone, film prepared by PS-PED method showed a high photocatalytic efficiency due to its high surface roughness and whiskered like structures. Whiskered like structures were developed routes for transferring of electrons and acted as structures for harvesting and multi-scattering of visible light. On the other hand, the nanofilm (13.78 nm) with high surface roughness on the conducting substrate contributed in separation of photogenerated hole-electron and increased the photocatalytic efficiency. To sum, pulse mode and sonication waves play key roles in synthesis of  $\text{Bi}_2\text{MoO}_6$  films due to overcoming the existing problems in electrodeposition method.

#### Acknowledgements

The support of Ferdowsi University of Mashhad (Research and Technology) is appreciated for this work (3/39052).

#### Appendix A. Supplementary data

Supplementary data to this article can be found online at <https://doi.org/10.1016/j.ultrsonch.2019.104867>.

#### References

- W.H. Organization, Pharmaceuticals in Drinking-water, WHO Libr. Cat. Data. WA 30.5 (2012) 35. doi:10.1331/JAPhA.2010.09186.
- R.P. Deo, R.U. Halden, Pharmaceuticals in the built and natural water environment of the United States, Water (Switzerland) 5 (2013) 1346–1365, <https://doi.org/10.3390/w5031346>.
- J. Rivera-Utrilla, M. Sánchez-Polo, M.Á. Ferro-García, G. Prados-Joya, R. Ocampo-Pérez, Pharmaceuticals as emerging contaminants and their removal from water. A review, Chemosphere 93 (2013) 1268–1287, <https://doi.org/10.1016/j.chemosphere.2013.07.059>.
- P. Grenni, V. Ancona, A. Barra Caracciolo, Ecological effects of antibiotics on natural ecosystems: a review, Microchem. J. 136 (2018) 25–39, <https://doi.org/10.1016/j.microc.2017.02.006>.
- R.M. Briones, A.K. Sarmah, L.P. Padhye, A global perspective on the use, occurrence, fate and effects of anti-diabetic drug metformin in natural and engineered ecosystems, Environ. Pollut. 219 (2016) 1007–1020, <https://doi.org/10.1016/j.envpol.2016.07.040>.
- J.L. Kormos, M. Schulz, T.A. Ternes, Occurrence of iodinated X-ray contrast media and their biotransformation products in the urban water cycle, Environ. Sci. Technol. 45 (2011) 8723–8732, <https://doi.org/10.1021/es2018187>.
- T.A. Ternes, R. Hirsch, Occurrence and behavior of X-ray contrast media in sewage facilities and the aquatic environment, Environ. Sci. Technol. 34 (2000) 2741–2748, <https://doi.org/10.1021/es991118m>.
- L.M. Madikizela, L. Chimuka, Occurrence of naproxen, ibuprofen, and diclofenac residues in wastewater and river water of KwaZulu-Natal Province in South Africa, Environ. Monit. Assess. 189 (2017) 348–360, <https://doi.org/10.1007/s10661-017-6069-1>.
- J. Bing, C. Hu, Y. Nie, M. Yang, J. Qu, Mechanism of catalytic ozonation in  $\text{Fe}_2\text{O}_3/\text{Al}_2\text{O}_3/\text{SBA-15}$  aqueous suspension for destruction of ibuprofen, Environ. Sci. Technol. 49 (2015) 1690–1697, <https://doi.org/10.1021/es503729h>.
- S.K. Ray, D. Dhakal, S.W. Lee, Rapid degradation of naproxen by AgBr-A-NiMoO<sub>4</sub> composite photocatalyst in visible light: mechanism and pathways, Chem. Eng. J. 347 (2018) 836–848, <https://doi.org/10.1016/j.cej.2018.04.165>.
- H. Kohay, A. Izbitski, Y.G. Mishaal, Developing polycation-clay sorbents for efficient filtration of diclofenac: effect of dissolved organic matter and comparison to activated carbon, Environ. Sci. Technol. 49 (2015) 9280–9288, <https://doi.org/10.1021/acs.est.5b01530>.
- J. Schwaiger, H. Ferling, U. Mallow, H. Wintermayr, R.D. Negele, Toxic effects of the non-steroidal anti-inflammatory drug diclofenac. Part I: Histopathological alterations and bioaccumulation in rainbow trout, Aquat. Toxicol. 68 (2004) 141–150, <https://doi.org/10.1016/j.aquatox.2004.03.014>.
- A. Inan, C. Koca, M. Şen, Effects of diclofenac sodium on bursting pressures of anastomoses and hydroxyproline contents of perianastomotic tissues in a laboratory study, Int. J. Surg. 4 (2006) 222–227, <https://doi.org/10.1016/j.ijssu.2006.01.002>.
- Z.K. El-Maddawy, I.M. El-Ashmawy, Hepato-renal and hematological effects of diclofenac sodium in rats, Glob. J. Pharmacol. 7 (2013) 123–132, <https://doi.org/10.5829/idosi.gjp.2013.7.2.72171>.
- W.H. Hörl, Nonsteroidal anti-inflammatory drugs and the kidney, Pharmaceuticals 3 (2010) 2291–2321, <https://doi.org/10.3390/ph3072291>.
- M.E. Simonsen, Heterogeneous Photocatalysis, Chem. Adv. Environ. Purif. Process. Water Fundam. Appl. (2014) 135–170, <https://doi.org/10.1016/B978-0-444-53178-0.00004-3>.
- A. Esmaeili, M.H. Entezari, Cubic Ag/AgBr-graphene oxide nanocomposite: sono-synthesis and use as a solar photocatalyst for the degradation of DCF as a pharmaceutical pollutant, RSC Adv. 5 (2015) 97027–97035, <https://doi.org/10.1039/c5ra16814g>.
- M. Khabbaz, M.H. Entezari, Degradation of Diclofenac by sonosynthesis of pyrite nanoparticles, J. Environ. Manage. 187 (2017) 416–423, <https://doi.org/10.1016/j.jenvman.2016.11.005>.
- J. Ângelo, P. Magalhães, L. Andrade, A. Mendes, Characterization of TiO<sub>2</sub>-based semiconductors for photocatalysis by electrochemical impedance spectroscopy, Appl. Surf. Sci. 387 (2016) 183–189, <https://doi.org/10.1016/j.apsusc.2016.06.101>.
- M. Khraishah, L. Wu, A.H. Al-Muhtaseb, A.B. Albadarin, G.M. Walker, Phenol degradation by powdered metal ion modified titanium dioxide photocatalysts, Chem. Eng. J. 213 (2012) 125–134, <https://doi.org/10.1016/j.cej.2012.09.108>.
- M. Paulose, H.E. Prakasam, O.K. Varghese, L. Peng, K.C. Papat, G.K. Mor, T.A. Desai, C.A. Grimes, TiO<sub>2</sub> nanotube arrays of 1000µm length by anodization of titanium foil: phenol red diffusion, J. Phys. Chem. C 111 (2007) 14992–14997, <https://doi.org/10.1021/jp075258r>.
- H. Zhao, F. Tian, R. Wang, R. Chen, A review on bismuth-related nanomaterials for photocatalysis, Rev. Adv. Sci. Eng. 3 (2014) 3–27, <https://doi.org/10.1166/rase.2014.1050>.
- X. Meng, Z. Zhang, Bismuth-based photocatalytic semiconductors: introduction, challenges and possible approaches, J. Mol. Catal. A, Chem. 423 (2016) 533–549, <https://doi.org/10.1016/j.molcata.2016.07.030>.
- L. Zhang, W. Wang, L. Zhou, H. Xu, Bi<sub>2</sub>WO<sub>6</sub> nano- and microstructures: shape control and associated visible-light-driven photocatalytic activities, Small 3 (2007) 1618–1625, <https://doi.org/10.1002/sml.200700043>.
- L. Zhou, W. Wang, L. Zhang, Ultrasonic-assisted synthesis of visible-light-induced Bi<sub>2</sub>MoO<sub>6</sub> (M = W, Mo) photocatalysts, J. Mol. Catal. A Chem. 268 (2007) 195–200, <https://doi.org/10.1016/j.molcata.2006.12.026>.
- W. Yin, W. Wang, S. Sun, Photocatalytic degradation of phenol over cage-like Bi<sub>2</sub>MoO<sub>6</sub> hollow spheres under visible-light irradiation, Catal. Commun. 11 (2010) 647–650, <https://doi.org/10.1016/j.catcom.2010.01.014>.
- P. Tao, Y. Xu, Y. Zhou, C. Song, Y. Qiu, W. Dong, M. Zhang, M. Shao, Nitrogen oxide (NO) gas-sensing properties of Bi<sub>2</sub>MoO<sub>6</sub> nanosheets synthesized by a hydrothermal method, Mater. Res. (2017) 2–6.
- J. Yang, Z. Ling, Y. Zhuang, Bi<sub>2</sub>MoO<sub>6</sub> dielectric thin films fabricated by thermal oxidation of Bi/Mo thin films at ultra-low temperature, J. Mater. Sci. Mater. Electron. 25 (2014) 1856–1862, <https://doi.org/10.1007/s10854-014-1810-9>.
- Y. Liu, F. Zhou, S. Zhan, Y. Yang, Preparation of Ag/AgBr-Bi<sub>2</sub>MoO<sub>6</sub> plasmonic photocatalyst films with highly enhanced photocatalytic activity, J. Inorg. Organomet. Polym. Mater. 27 (2017) 1365–1375, <https://doi.org/10.1007/s10904-017-0590-0>.
- J. Bi, L. Wu, J. Li, Z. Li, X. Wang, X. Fu, Simple solvothermal routes to synthesize nanocrystalline Bi<sub>2</sub>MoO<sub>6</sub> photocatalysts with different morphologies, Acta Mater. 55 (2007) 4699–4705, <https://doi.org/10.1016/j.actamat.2007.04.034>.
- L. Xie, J. Ma, G. Xu, Preparation of a novel Bi<sub>2</sub>MoO<sub>6</sub> flake-like nanophotocatalyst by molten salt method and evaluation for photocatalytic decomposition of rhodamine B, Mater. Chem. Phys. 110 (2008) 197–200, <https://doi.org/10.1016/j.matchemphys.2008.01.035>.
- V. Umaphathy, A. Manikandan, S. Arul Antony, P. Ramu, P. Neeraja, Structure morphology and opto-magnetic properties of Bi<sub>2</sub>MoO<sub>6</sub> nano-photocatalyst synthesized by sol-gel method, Trans. Nonferrous Met. Soc. China (English Ed.) 25 (2015) 3271–3278, [https://doi.org/10.1016/S1003-6326\(15\)63948-6](https://doi.org/10.1016/S1003-6326(15)63948-6).
- A. Martínez-De La Cruz, S. Obregón Alfaro, S.M.G. Marcos Villarreal, Photocatalytic behavior of α-Bi<sub>2</sub>Mo<sub>3</sub>O<sub>12</sub> prepared by the Pechini method: degradation of organic dyes under visible-light irradiation, Res. Chem. Intermed. 36 (2010) 925–936, <https://doi.org/10.1007/s11164-010-0205-7>.
- M. Zargazi, M.H. Entezari, Anodic electrophoretic deposition of Bi<sub>2</sub>WO<sub>6</sub> thin film: high photocatalytic activity for degradation of a binary mixture, Appl. Catal. B Environ. 242 (2019) 507–517, <https://doi.org/10.1016/j.apcatb.2018.09.093>.
- M. Zargazi, M.H. Entezari, BFO thin film on the stainless steel mesh by anodic EPD: a visible light photocatalyst for degradation of Rhodamine B, J. Photochem. Photobiol. A Chem. 365 (2018) 185–198, <https://doi.org/10.1016/j.jphotochem.2018.07.042>.
- M. Ratova, P. Kelly, G. West, X. Xia, Y. Gao, Deposition of visible light active photocatalytic bismuth molybdate thin films by reactive magnetron sputtering, Materials (Basel) 9 (2016) 67–80, <https://doi.org/10.3390/ma9020067>.
- E.L. Cuéllar, A.M. Cruz, K.H.L. Rodríguez, U.O. Méndez, Preparation of -Bi<sub>2</sub>MoO<sub>6</sub> thin films by thermal evaporation deposition and characterization for photocatalytic applications, Coatings 166 (2011) 140–145, <https://doi.org/10.1016/j.cattod.2010.05.005>.
- F. Zheng, G. Li, X. Yu, Y. Tong, Synthesis of Bismuth molybdate nanowires via electrodeposition – heat-treatment method, Electrochem. Solid-State Lett. (2014) 10–13, <https://doi.org/10.1149/1.3143909>.
- M. Zargazi, M.H. Entezari, Sonochemical versus hydrothermal synthesis of bismuth tungstate nanostructures: photocatalytic, sonocatalytic and sonophotocatalytic activities, Ultrason. Sonochem. 51 (2019) 1–11, <https://doi.org/10.1016/j.ultrsonch.2018.10.010>.